Available online at www.sciencedirect.com
ScienceDirect
Journal of Molecular Spectroscopy 249 (2008) 14–22
Journal of MOLECULAR SPECTROSCOPY
www.elsevier.com/locate/jms

Continuous-wave cavity ringdown spectroscopy of the N_2^+ Meinel system (2, 1) band

Susanna L. Widicus Weaver, Michael B. Wiczer, Bogdan Negru [1], Joshua P. DiGangi [2], Brian A. Tom, Benjamin J. McCall *

Departments of Chemistry and Astronomy, University of Illinois at Urbana-Champaign, Urbana, IL 61801, USA

Received 11 September 2007; in revised form 4 December 2007
Available online 4 March 2008

Abstract

The $A^2\Pi_u$–$X^2\Sigma_g^+$ system of N_2^+ was first observed in auroral emissions by Meinel in 1950. Although the N_2^+ band system has been reinvestigated since this first spectral study, no laboratory spectrum of the (2, 1) vibronic band has been obtained. We have recently built a continuous-wave cavity ringdown spectrometer, and as a first test of this spectrometer we observed the (2, 1) band of N_2^+ in a positive column discharge cell. Many lines of the first positive band system of N_2^* were also identified during the process of assigning this spectrum. The relative intensities of the N_2^* and N_2^+ bands were found to change with discharge cell pressure, and so each spectral region was observed at two pressures to aid in distinguishing the spectra of the two species. We have assigned 125 N_2^+ lines and determined the molecular parameters for the (2, 1) band from these assignments. The analysis of the N_2^* spectrum is ongoing and will be presented in a follow-up paper. The N_2^+ (2, 1) band transition frequencies predicted from available literature values vary significantly from our assignments. The observed deviations indicate correlation of other parameters with the spin-rotation parameter and the quartic centrifugal distortion constants. These results indicate that rovibronic predictions for new N_2^+ bands based on the parameters derived from individual band assignments are likely to be unreliable, and further investigation of the Meinel system may require a global analysis that accounts for this correlation.

Keywords: Nitrogen molecular ion; N_2^+; Meinel system; Near infrared; High-resolution infrared spectroscopy; Cavity ring down spectroscopy; CRDS

1. Introduction

The N_2^+ cation is important in atmospheric aurorae and is a common constituent of electrical discharges [1]. The $A^2\Pi_u$–$X^2\Sigma_g^+$ system of N_2^+ has been extensively studied spectroscopically, both in atmospheric and laboratory studies. Childs first proposed the existence of the $A^2\Pi_u$ excited state in 1932 [2], and this was confirmed by Meinel eighteen years later while observing auroral emissions in the near-infrared [3]. The $A^2\Pi_u$–$X^2\Sigma_g^+$ system became known as the Meinel system, and Dalby and Douglas began the laboratory characterization of this system in 1951 [4]. Assignments for seventeen Meinel system vibronic bands have been reported in the literature (see reference [5] and references therein).

We have recently constructed a near-infrared continuous-wave cavity ringdown spectrometer for the high resolution spectroscopic study of molecular ions based on the design of Romanini et al. [6]. This highly sensitive absorption technique relies on the use of a high finesse optical cavity to increase the absorption pathlength. The CRDS technique is not sensitive to intensity fluctuations because the rate of decay of light, rather than the magnitude, is measured. The combination of these two factors makes cw-CRDS a powerful tool for detection of gas phase species with weak spectral features, such as molecular ions.

* Corresponding author.
E-mail address: bjmccall@uiuc.edu (B.J. McCall).
[1] Present address: Department of Chemistry, University of California, Berkeley, USA.
[2] Present address: Department of Chemistry, University of Wisconsin, Madison, USA.

0022-2852/$ - see front matter © 2008 Elsevier Inc. All rights reserved.
doi:10.1016/j.jms.2007.12.002

Indeed, near-IR cw-CRDS experiments have achieved absorbance baseline RMS levels on the order of 10^{-11} cm^{-1} [7]. We refer the reader to reference [8] for a general review of CRDS techniques.

The tunable external cavity diode laser used with our spectrometer covers the wavelength range of the N_2^+ (2,1) vibronic band, and so this band was used to test the spectrometer and calibration routines. The N_2^+ (2,1) band has never before been observed in the laboratory, and only a few studies provide high accuracy N_2^+ data in the 9000 to 14500 cm^{-1} range [9]. To improve upon previous studies, we present here the laboratory spectroscopic study and analysis of the N_2^+ (2,1) vibronic band between 10227 and 10590 cm^{-1}.

2. Experimental design

The experimental technique employed was near-infrared continuous-wave cavity ringdown spectroscopy (cw-CRDS), and the spectrometer design is shown in Fig. 1. The Sacher Lasertechnik Lion external cavity diode laser used was tunable over the 922–985 nm range and the single-mode output power of the laser at 965 nm was >100 mW. The short-term laser linewidth specified by the manufacturer was <300 kHz. The diode laser beam was split into a reference beam and a signal beam by a 50/50 beamsplitter. The signal beam was passed through an acousto-optic modulator [AOM; Brimrose, TEM-85-2 (AOM) and FFA-85-B2-F2.25-X (driver)], and the first order diffraction (~70% of

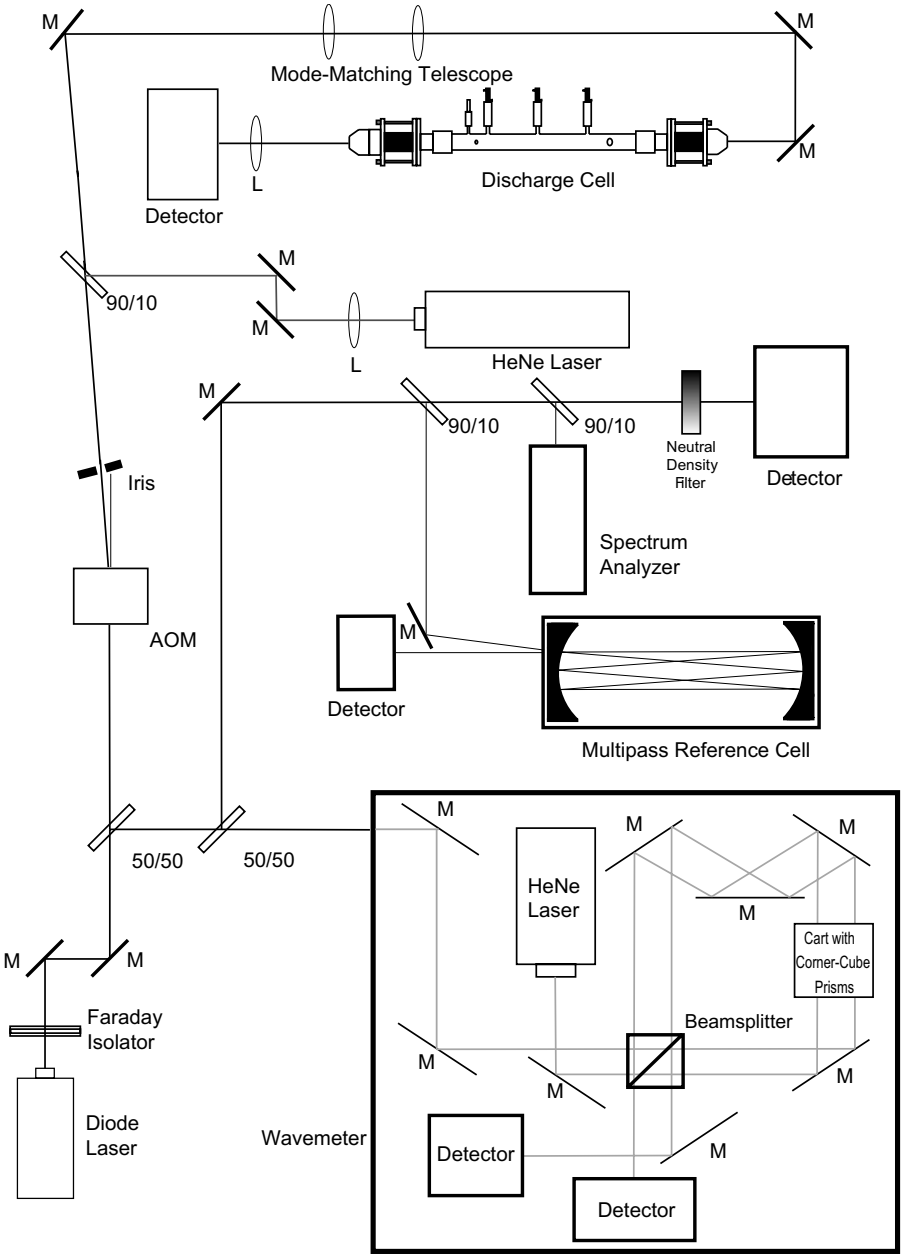

Fig. 1. Schematic diagram of the continuous-wave cavity ringdown spectrometer.

the incident beam power) was selected with an iris. The signal beam was then made collinear with the output from a 0.5 mW HeNe laser introduced through a 90/10 beamsplitter to aid in alignment. An optical telescope was used to mode match the signal beam with the TEM_{00} mode of a high finesse cavity. The cavity was comprised of two high reflectivity mirrors (Los Gatos Research, 901-0010-0950) with $R = 0.99982$ as determined from the observed baseline ringdown time ($R = 0.9999$ was specified by the manufacturer). The mirrors had a center wavelength of 950 nm, a radius of curvature of 1 m, and anti-reflection coatings (on the non-HR side) with a residual reflectivity of 0.05%. The mirror transmission specified by the manufacturer was 0.009–0.022% across the laser tuning range.

The cavity mirrors were placed at each end of a glass discharge cell at a separation of 110 cm. The mirrors were mounted in home-built stainless steel mirror mounts with precision alignment screws allowing for three-axis adjustment of the mirror position. In addition, one mirror was attached to a piezoelectric crystal (Piezomechanik, HPSt 150/20-15/12 VS35) used to dither the cavity in and out of resonance with the laser. The power transmitted out of the cavity was recorded with a silicon avalanche photodiode detector (Hamamatsu, APD C5460), and this signal was monitored with a comparator circuit. When a given threshold intensity was reached, the TTL output of the comparator switched to low, modulating the amplitude of the RF drive to the AOM. This suppressed the optical power of the first order diffraction by at least −42 dB, allowing ringdown to occur.

A LabWindows data acquisition routine utilizing a 100 MHz, 14 bit high speed digitizer card recorded the exponential decay of each ringdown event. The decay time constant was calculated for each ringdown using a fast exponential fitting algorithm [10], and time constants for 10 ringdowns as well as 100 readings for each reference signal were collected at each scan step. A box-and-whiskers routine selected the readings within the middle 50% of the data spread, and the average value of these was recorded. Typical ringdown transients had a signal-to-noise ratio of >150, and the incident power on the detector at the peak of a ringdown transient was typically >0.7 μW. During scanning, the voltage applied to a piezo actuator in the laser was stepped in 0.01 V increments, adjusting the angle of the end mirror in the external cavity, which in turn tuned the laser output frequency by $\sim 0.004\ cm^{-1}$ per scanning step. Each scan was comprised of 1000 steps and covered $\sim 4\ cm^{-1}$. The typical acquisition rate was >100 ringdown transients s^{-1}. The minimum detectable absorbance (α_{min}) observed was $2 \times 10^{-9}\ cm^{-1}$, which corresponds to the peak-to-peak noise of the baseline while averaging 100 ringdown events per point. The RMS baseline noise observed during scanning while averaging 100 ringdowns per point was $5 \times 10^{-10}\ cm^{-1}$, and a comparable noise level was observed for 100 ringdowns acquired in the absence of laser scanning. The baseline ringdown time was between 10 and 20 μs and decreased steadily with an increase in frequency across the scanning region.

The reference beam was monitored by several instruments for the purpose of spectral calibration. Two 90/10 beamsplitters were used to couple the reference beam into a wavemeter, a spectrum analyzer, and a Herriott cell. A picometer-resolution wavemeter was used for rough frequency calibration and for identifying the length of mode hops that occurred during scanning. This home-built traveling wavemeter design was based on the theory of Michelson interferometry adapted to work with visible/NIR lasers [11]. The wavemeter consisted of two corner-cube prisms placed on a movable cart, thus halving the distance that the prisms needed to travel to collect sufficient fringes for wavelength determination. Cart automation and a computer interface for data acquisition were implemented for this experiment [12].

In addition to the wavemeter, a 1.5 GHz Thorlabs high finesse spectrum analyzer was used in conjunction with an etalon finder circuit to detect mode hops. The etalon finder circuit was based on the design used by the Oka group [13], which was in turn based on the designs of reference [14] and references therein. A ramp voltage was applied to the piezoelectric element in the spectrum analyzer, and the output signal of the spectrum analyzer peaked when its cavity was in resonance with the laser frequency. The ramp voltage at which resonance was achieved changed as the laser scanned in frequency, and the etalon finder monitored this voltage. In the absence of mode hops, the etalon finder signal was a smoothly varying saw-tooth with respect to the laser tuning voltage, as is shown in Fig. 2. A discontinuity in this saw-tooth indicated a mode hop, and simultaneous measurement of the wavemeter signal provided the necessary information for determining the number of free spectral ranges hopped and was used for frequency extrapolation across the mode hop. The combined drift rate of the etalon and laser was $0.0001\ cm^{-1}\ s^{-1}$, and the 1-σ RMS of the etalon finder signal at a fixed laser piezo actuator voltage corresponded to a short-term frequency uncertainty of $0.0003\ cm^{-1}$.

Absolute frequency calibration was obtained with the use of a multi-pass Herriott cell providing a direct absorption pathlength of ~40 m. The cell was filled with water vapor to a pressure of 16 mTorr. The scanning ranges were adjusted to allow for observation of at least one water line in each scan, and two or more lines were observed in most frequency windows. Each water line was fit to a Gaussian, and the line center position was assigned to the HITRAN frequency for the line [15]. The etalon finder and wavemeter information were then used to interpolate the frequencies between observed water lines. A fit of the etalon free spectral range to the calibration lines gave a 1-σ frequency uncertainty of $0.004\ cm^{-1}$, which corresponds to the frequency calibration accuracy. Also, several lines were observed in more than one cavity ringdown spectrum, and an estimate of the frequency calibration precision was made from comparison of the center frequencies of

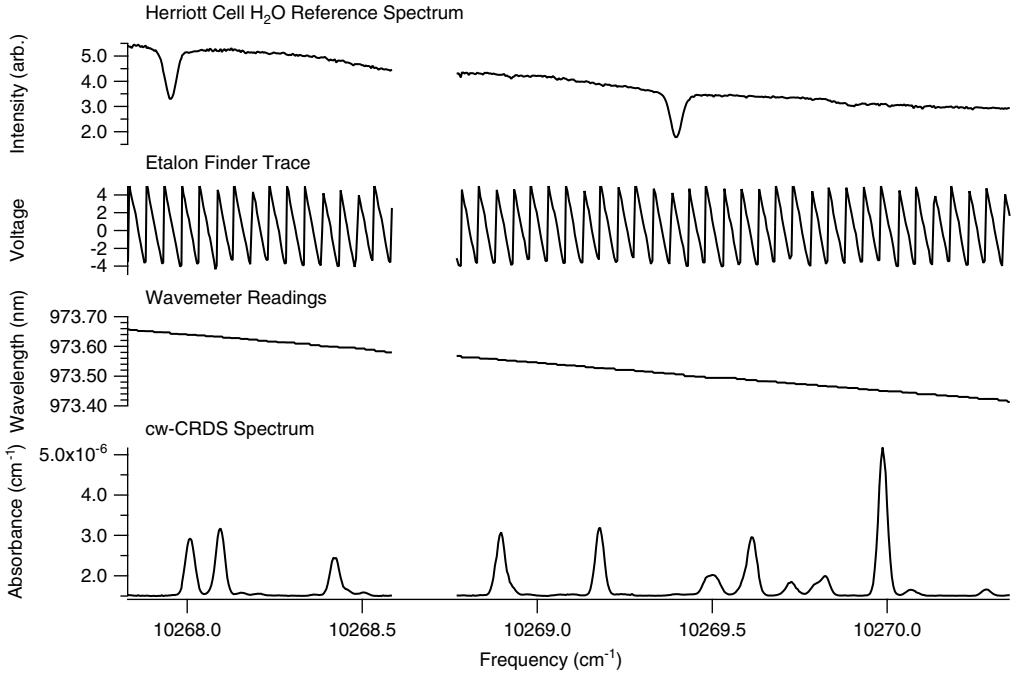

Fig. 2. Example spectrum showing the reference spectrum of water, etalon finder signal, wavemeter output, and cw-CRDS spectrum. The discontinuity at 10268.6 cm^{-1} corresponds to a mode hop.

these lines. This analysis indicated that the frequency calibration precision for N_2^+ lines was typically much better than the frequency calibration accuracy.

Atmospheric water absorption lines are quite strong in this frequency region, and the laser tended to mode hop at frequencies near these lines. Additional, smaller mode hops were prevalent throughout the scans, indicating that the diode laser did not have a wide mode hop-free scanning range. The frequency calibration could in most cases be extrapolated across the mode hops, allowing for calibration of all spectral segments. However, many predicted N_2^+ (2, 1) band lines were missed entirely because of mode hops. Adjustment of the laser current coupling and purging of the laser cavity with dry nitrogen may eliminate some mode hops, but it is unclear whether either type of mode hop can be entirely eliminated for this particular laser.

The N_2^+ molecular ions were produced in an 88 cm long positive column discharge cell designed for cw-CRDS. Three water-cooled electrodes were spaced along the length of the cell at a separation of 20.3 cm, and the cavity ring-down mirrors were mounted at the ends of the cell. The discharge was struck between the middle and one of the outer electrodes, and the mirror mounts were grounded to reduced unwanted arcing in the vicinity of the mirrors. Two 10 kΩ ballast resistors were connected in series with the middle lead, and the voltage was fixed at a value near −3100 V that produced a discharge current of 70 mA, as this was found to maximize the N_2^+ signal. A curtain of argon gas protected the mirrors and provided a background cell pressure of 300 mTorr. Nitrogen gas was then introduced to increase the total cell pressure to either 500 mTorr or 3 Torr. The system was used as a flow cell and constant pressure was maintained with a Duo-Seal Welch vacuum pump. The flow rate was limited to 0.1 L s^{-1} by the tubing used to connect the discharge cell to the vacuum pump.

Lines from the $B^3\Pi_g$–$A^3\Sigma_u^+$ first positive group of N_2 increased the observed spectral complexity. Several N_2 first positive group bands, specifically the (2, 2), (3, 3), (4, 4), (5, 5), (7, 8), and (8, 9) bands, have strong lines in this spectral region [16]. Both the N_2^+ and N_2^* peak intensities were found to vary significantly with pressure, as is shown in Fig. 3. While the N_2^+ lines increased in intensity with an increase in pressure, the N_2^* lines decreased in intensity with an increase in pressure. The N_2^* line intensity decrease

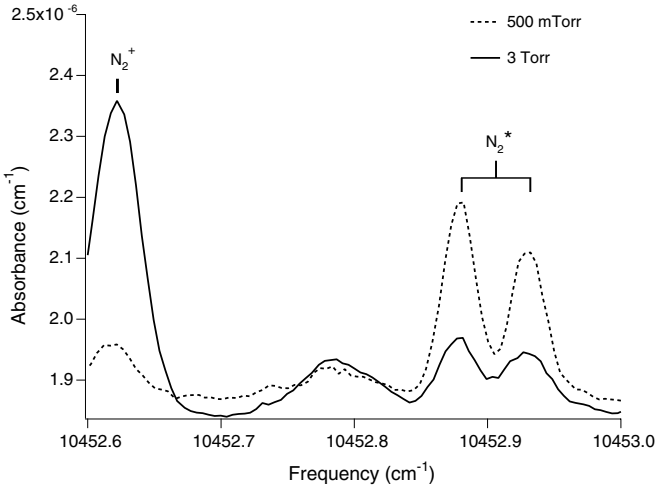

Fig. 3. Comparison of the N_2^+ and N_2^* spectra at two different discharge pressures.

likely arose from collisional deexcitation of the metastable N_2 at higher pressures, as was observed for H_2^* in similar experiments [17]. Spectra were therefore recorded at 500 mTorr and 3 Torr to aid in the identification of N_2^+ lines. Comparison of the spectra taken at 500 mTorr and 3 Torr allowed for the assignment of spectral features to either N_2^* or N_2^+ (see Fig. 3).

3. Theory

The Meinel system of N_2^+ consists of transitions between the $A^2\Pi_u$ and $X^2\Sigma_g^+$ electronic states. The A–X transitions observed here are not perturbed by any higher energy states since the $v = 0$ level of the B state, the next lowest energy state, is above the $v = 9$ level of the A state [18]. Initial spectral predictions were based on the effective Hamiltonians of Miller et al. [18] and Ferguson et al. [1], and the relative intensities of each transition were calculated with the intensity formulas of Earls [19]. Molecular parameters from Ho et al. [20] for $v' = 2$ and Ferguson et al. [1] for $v'' = 1$ were used to predict the vibronic frequencies for the (2,1) band transitions at 1000 K, and the predicted N_2^+ spectrum is shown in Fig. 4. This prediction was used as a guide for assignment of the observed spectrum. Our final spectral analysis used the nonlinear least-squares fitting routine of Tarsitano and Oka [5].

The Hamiltonians used in the spectral analysis [5] were equivalent to the effective Hamiltonians used for the prediction [18]. We refer the reader to these studies for a detailed discussion of these Hamiltonians, and present only the following brief description. The $X^2\Sigma_g^+$ state displays regular spin–orbit coupling and follows Hund's case (b), with the spin components F_1 and F_2 corresponding to $J = N + 1/2$ and $J = N - 1/2$, respectively. The standard Hund's case (b) Hamiltonian was used, and this Hamiltonian includes molecular parameters for the vibronic energy ($T_{v''}$), the rotational constant ($B_{v''}$), the quartic centrifugal distortion constant ($D_{v''}$), and the spin-rotation constant (γ). The $A^2\Pi_u$ state displays inverted spin–orbit coupling and follows Hund's case (a). Lambda doubling couples with centrifugal distortion, leading to a much more complicated Hamiltonian than that used for the $X^2\Sigma_g^+$ state. Additional molecular parameters include the spin–orbit coupling constant ($A_{v'}$), the centrifugal distortion of the spin–orbit constant ($A_{Jv'}$), and effective lambda doubling constants ($p_{v'}$ and $q_{v'}$). The value of $A_{Jv'}$ is half of the value of the parameter $A_{Dv'}$ used in references [1,18,20].

4. Results and analysis

The $A^2\Pi_u$–$X^2\Sigma_g^+$ (2,1) band of N_2^+ was recorded in the 10227–10587 cm^{-1} range, where more than 575 absorption lines with an average line width of 0.03 cm^{-1} have been identified. The complete spectra at each pressure are shown in Fig. 5.

Out of >575 observed lines, 125 have been positively assigned to the previously unobserved N_2^+ (2, 1) band using the prediction shown in Fig. 4. All assigned N_2^+ (2,1) band lines are shown in Fig. 4 and listed by branch in Table 1. A total of 400 N_2^+ (2,1) band lines are predicted for this frequency range, but only 241 of these are of sufficient intensity to be detected in this experiment. Of those lines that should be observable, 60 are coincident in frequency with mode hops, and 56 cannot be discerned from strong N_2 first positive group lines. No lines were observed from

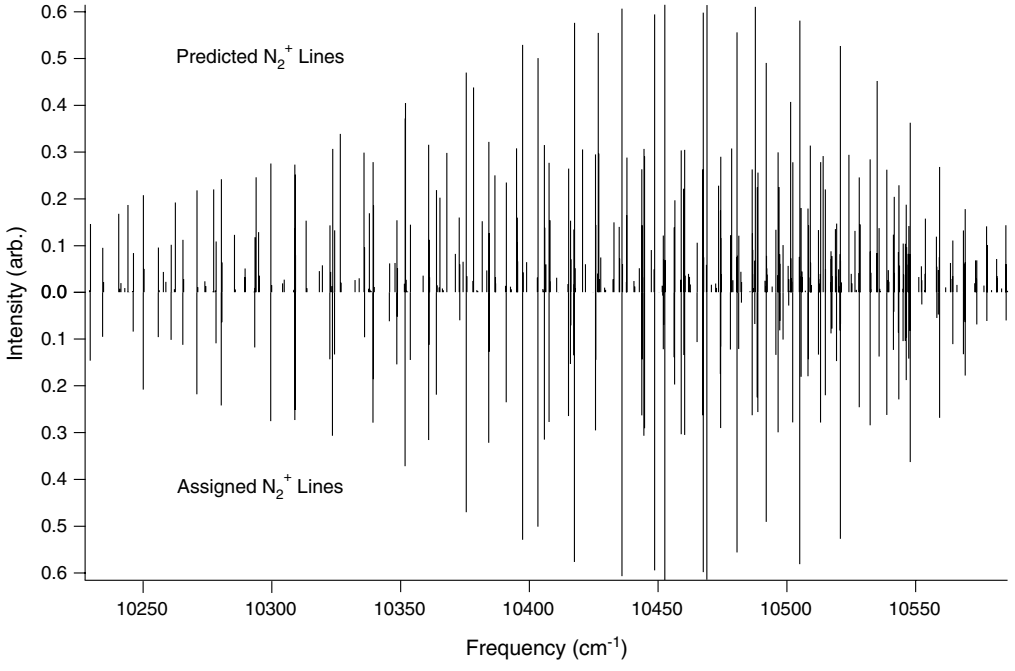

Fig. 4. Stick spectra showing the assigned and predicted lines of N_2^+.

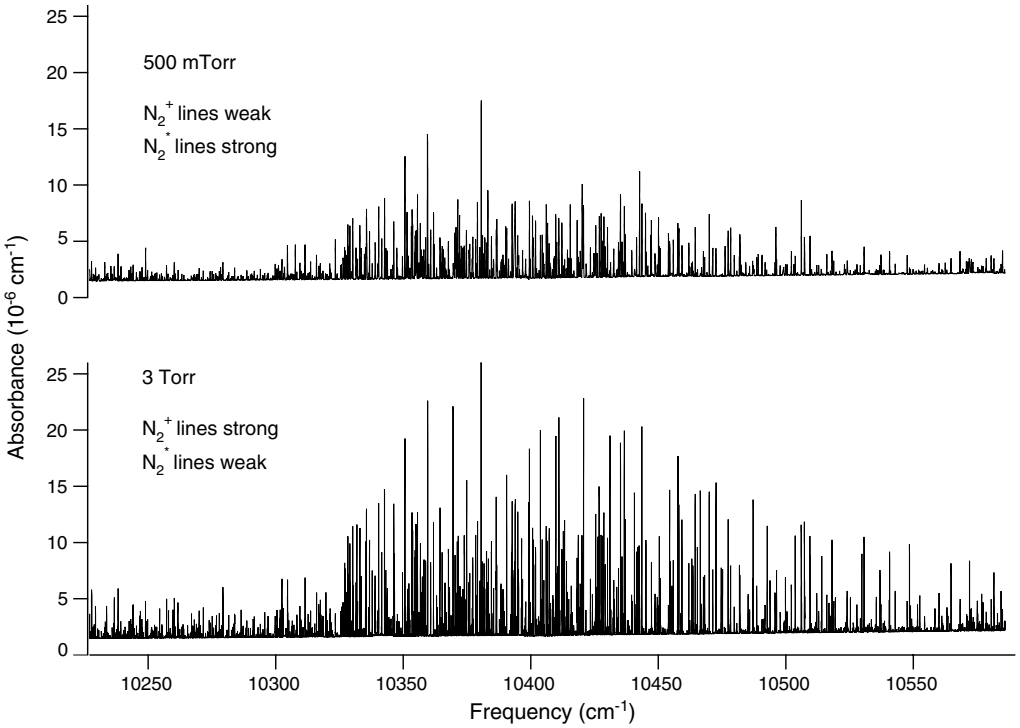

Fig. 5. Complete spectra at 500 mTorr and 3 Torr.

the N_2^+ P_{12}, R_{21}, or R_{12} subbands. Each observed N_2^+ line was fit to a Gaussian lineshape for line center frequency determination, and multiple Gaussians were used in cases of partially blended lines.

In the process of assigning the (2,1) Meinel System band, more than 450 N_2 first positive group lines have also been tentatively assigned. The N_2^* line density was much greater than that of the corresponding molecular ion, and the line intensities were also significantly greater in most cases. Analysis of this spectrum is ongoing, and the results will be reported separately.

The molecular parameters determined from the N_2^+ spectral analysis are given in Table 2. The 1-σ RMS of the spectral fit is 0.0071 cm^{-1}, which is approximately twice the scanning step size and one quarter of the observed linewidth. The Hamiltonians used for the rotational analysis are described above, and the fitting routine was a nonlinear least-squares fit performed with the Mathematica® NonlinearRegress function [21]. The value of γ is strongly correlated with the rest of the molecular parameters, but can be obtained separately from combination differences between the R_{22}–Q_{21}, Q_{22}–P_{21}, and Q_{12}–P_{11} subbands. These combination differences were plotted versus the quantum number N, resulting in a line with slope equal to γ. The value of γ was then fixed in the least squares fit for determination of the additional molecular parameters.

As shown in Table 2, our determined molecular parameters are generally within 2-σ of the values reported in other studies, and the uncertainties of our values are comparable to those previously reported. However, it should be noted that our value of $D_{v''}$ varies from that reported in reference [1], and that many of the values reported in reference [9] vary significantly from both our determined values and those of the other studies. To further explore these discrepancies, we calculated the observed–calculated residuals using the assigned frequencies from this work and the parameters reported in the other studies listed in Table 2. The results of this analysis are shown in Fig. 6. Clearly there is a strong linear N-dependence in the residuals when the parameters from other studies are used, and an additional quadratic dependence arises from the parameters given in reference [9]. This trend is also observed when the assignments of reference [5] are analyzed in a similar manner. We suspect that the linear dependence arises from the highly correlated nature of the spin-rotation constant, as is discussed in reference [5]. The quadratic dependence is likely from correlation of other parameters with one or both of the quartic centrifugal distortion constants. Such correlations between parameters have been noted in other studies [5,18]. The results shown in Fig. 6 indicate that rovibronic predictions for N_2^+ based on the parameters derived from individual band assignments are likely to provide unreliable frequency predictions for other bands, and further investigation of the Meinel system may require a global analysis that accounts for this correlation.

In addition to the improvement of the molecular parameters for the (2,1) band of N_2^+, this experiment allowed us to test the capabilities of our newly constructed spectrometer and the reliability of our calibration routines. The achieved frequency calibration accuracy of 0.004 cm^{-1}, or 120 MHz, is more than sufficient for Doppler-limited spectroscopic studies in the near-IR. The greatest contribution

Table 1
Assigned N_2^+ (2, 1) band transition center frequencies in cm^{-1}

N	P_{11}	P_{21}	P_{22}	Q_{11}	Q_{12}	Q_{21}	Q_{22}	R_{11}	R_{22}
1				W				W	
2	W		W	W	W			W	
3	W		W	W	W			W	
4	MH	W	W	10520.8596(85)	W		W	W	
5	W	W	W	MH	W		W	W	
6	10497.2410(-43)	W	10558.8242(8)	B	10497.3146(1)		MH	W	
7	MH	W	MH	10517.1301(35)	W		10573.7501(11)	B	
8	MH	10569.2125(44)	10543.3361(−10)	10514.9281(−53)	MH		10569.2911(39)	10546.4995(−15)	
9	B	W	MH	10512.2655(−32)	B		10564.4750(−13)	MH	
10	10474.1989(−77)	MH	MH	MH	10474.3035(13)		10559.3147(11)	10547.3533(−37)	
11	MH	MH	10517.4964(−77)	10505.5341(−13)	B		MH	MH	
12	MH	10547.8067(11)	10508.1923(31)	MH	10459.9758(−60)		10547.9197(−23)	10546.3608(101)	
13	10452.0089(66)	10541.5642(23)	10498.5124(−56)	MH	10452.1252(−02)		MH	10545.1548(−8)	
14	10443.6835(55)	MH	10488.4881(3)	10491.9693(15)	10443.8090(−13)	B	MH	10543.4965(−62)	10585.1659(39)
15	B	B	10478.0917(−44)	10486.5309(−5)	MH	W	10528.1288(7)	10541.3918(−25)	B
16	10425.6645(22)	10520.6452(11)	10467.3359(−44)	10480.6423(−3)	10425.8224(94)	MH	10520.7989(12)	10538.8380(51)	10577.6991(5)
17	10415.9736(−29)	B	10456.2143(−37)	10474.3035(−8)	10416.1329(−34)	W	10513.1038(70)	10535.8295(89)	B
18	10405.8316(−106)	B	10444.7259(−6)	10467.5252(78)	B	10568.5612(30)	10505.0241(14)	10532.3549(−47)	10568.7285(−20)
19	B	B	B	10460.3023(168)	MH	W	10496.5841(107)	MH	MH
20	10384.2357(−23)	10487.5557(0)	B	10452.6215(111)	10384.4280(25)	MH	MH	B	10558.2259(−124)
21	B	B	MH	10444.4937(−3)	10372.9616(−72)	W	MH	10519.2981(−56)	10552.4102(−50)
22	10360.8577(−109)	MH	B	10435.9439(56)	10361.0686(−59)	10546.2003(−44)	10468.9532(15)	B	10546.2003(−44)
23	10348.5289(17)	W	B	MH	10348.7438(14)	W	10458.9763(−37)	10508.3829(−69)	MH
24	MH	W	MH	10417.5259(100)	10335.9782(31)	W	10448.6251(21)	10502.2723(−22)	MH
25	10322.5348(−62)	W	10353.7780(33)	10407.6610(85)	B	W	B	10495.7295(75)	B
26	10308.9004(8)	W	10339.2564(−15)	10397.3600(36)	MH	W	MH	10488.7319(−18)	B
27	MH	W	10324.3572(19)	B	W	W	10415.2194(−53)	10481.3044(64-)	MH
28	10280.3309(26)	W	10309.0591(−70)	10375.4750(42)	10280.6119(189)	W	10403.3137(24)	MH	10500.7061(−29)
29	10265.4048(34)	W	10293.3688(−199)	10363.8916(76)	W	W	10391.0122(66)	10465.1413(−236)	MH
30	10250.0577(90)	W	B	B	MH	W	MH	10456.4239(−199)	10482.3770(52)
31	10234.2774(57)	W	10260.8807(151)	10339.4267(−10)	W	W	B	B	B
32		W	B	B		W	10351.7262(30)	MH	B
33		W		B		W	B	MH	10451.8806(218)
34		W		10299.5314(−202)		W	10323.5502(−38)	10417.2601(21)	B
35		W		B		W	10308.8785(59)	MH	W
36		W		10270.8468(−27)		W	B	B	MH
37		W		10255.8712(58)		W	10278.3166(39)	W	W
38		W		W		W	B	B	W
39		W				W	10246.1459(−64)	W	W
40		W				W	10229.4551(−154)	10345.6552(120)	W

'MH' denotes lines that were not observed due to laser mode hops, 'B' denotes lines that were blended with or obscured by stronger N_2 lines, and 'W' denotes lines that were weaker than our detection limit. Those transitions with no entry occur outside of the experimental frequency range. All transitions with $N > 40$ were either too weak to be observed in our experiment, or occur outside of the experimental frequency range. The observed–calculated frequency residuals are listed in parentheses in units of the last significant digit.

Table 2
Molecular parameters (in cm^{-1}) determined for the (2,1) band of N_2^+

Parameter	This work	Refs. [1,20]	Ref. [18]	Ref. [9]
$T_{v'v''}$	10558.0905(17)	10558.0911[a]		
$B_{v'}$	1.697246(49)	1.697391(67)	1.697305(19)	1.6973673(17)
$D_{v'} \times 10^6$	5.760(33)	5.91(10)	5.830(31)	5.9319(14)
$A_{v'}$	−74.6294(29)	−74.6332(18)	−74.6214(41)	−74.63666(73)
$A_{Jv'} \times 10^5$	−3.50(29)	−4.0(11)	−5.00(70)	−0.303(9)
$q_{v'} \times 10^4$	−3.298(34)	−3.08(11)[b]	−3.08(11)	−3.336(13)
$p_{v'} \times 10^3$	4.889(12)	4.87(27)[b]	4.87(27)	5.017(44)
$B_{v''}$	1.903298(51)	1.903373(13)	1.903350(29)	1.903300(20)
$D_{v''} \times 10^6$	5.804(35)	5.942(8)	5.909(48)	5.904(21)
$\gamma \times 10^3$	9.31(11)	9.197(27)	8.63(22)	9.156(43)
RMS	0.0071			

The 1-σ uncertainties listed in parentheses are in units of the last significant digit.
[a] No uncertainty was reported for this value.
[b] These values were fixed to those reported in Ref. [18].

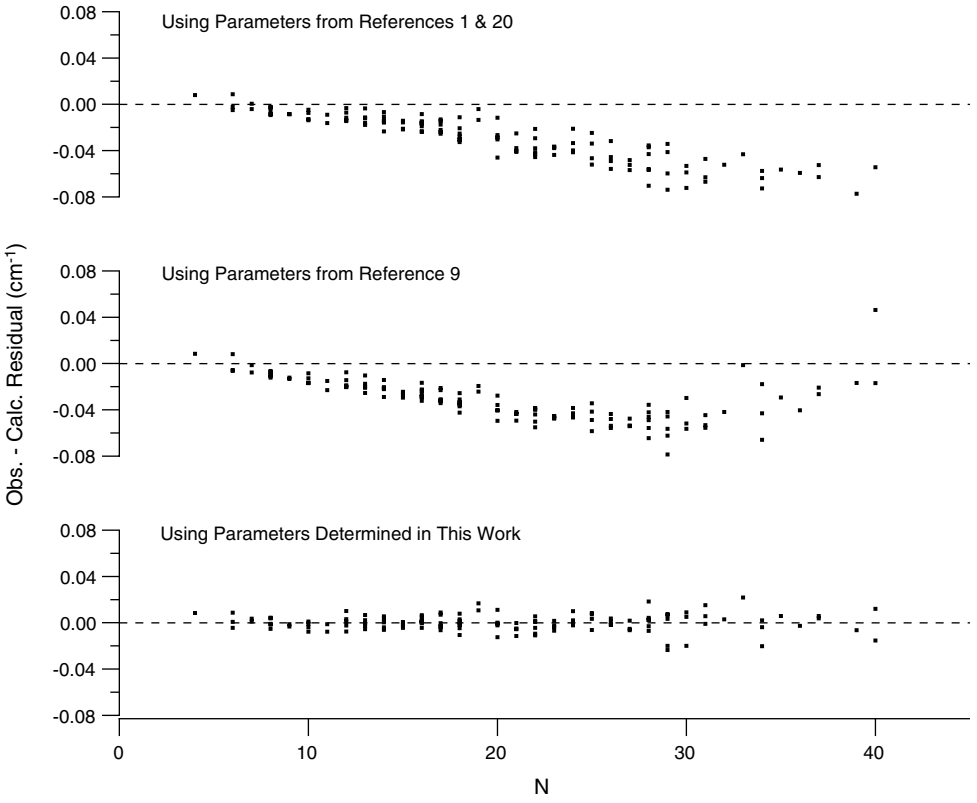

Fig. 6. Comparison of the observed–calculated residuals versus N using the parameters determined from other studies and those determined in this work.

to uncertainty in the spectral fit was from the uncertainty in the center position of the calibration lines, which arose from pressure broadening. Nonetheless, the frequency calibration accuracy is equal to the scanning step size, which is quite reasonable for this experimental setup. Lower reference cell pressures might be used in future experiments to reduce the contribution to the uncertainty from pressure broadening.

The ringdown baseline RMS of 5×10^{-10} cm^{-1} is a factor of 2.7 higher than that achieved in a similar near-IR experiment [7]. Most of this discrepancy can be accounted for by comparison of the quality of the ringdown mirrors—those used by Dudek et al. [7] yielded at least a factor of two longer ringdown times than achieved in our experiment. Other possible sources of baseline noise include the occasional excitation of cavity modes other than the TEM_{00} mode as well as insufficient suppression of the first order beam by the AOM. Baseline RMS values of 10^{-11} cm^{-1} are now commonly achieved in near-IR cw-CRDS experiments, and so our setup can certainly be improved. For comparison, we consider Dudek et al. [7], where two major improvements over our cw-CRDS setup were implemented: higher quality mirrors yielding ringdown times as long as 300 μs were used, and the laser drive

current was modulated. We plan to explore these options as well as high-repetition-rate cw-CRDS techniques [22] so as to enable detection of even weaker spectral features.

5. Conclusion

A high resolution spectrum of the previously unobserved N_2^+ $A^2\Pi_u$–$X^2\Sigma_g^+$ (2,1) band has been obtained and 125 N_2^+ lines have been assigned. Molecular parameters were calculated from these assignments, yielding an RMS for the spectral fit of 0.0071 cm^{-1} which corresponds to one quarter of the linewidth. A high degree of correlation between the molecular parameters was observed, and deviations were observed when these assignments were compared to predictions based on previously reported molecular parameters. Reliable predictions of other N_2^+ Meinel system bands may require further global analysis with methods that independently determine the highly correlated parameters.

In addition to the N_2^+ assignments, more than 450 lines from the first positive band system of N_2 have also been observed. Analysis of these results is ongoing and will be reported separately.

This project demonstrates the capabilities of our newly constructed continuous-wave cavity ringdown spectrometer. The spectral calibration routines developed for this study enable highly accurate frequency determination sufficient for Doppler-limited near-IR spectroscopic studies. Although the sensitivity can be improved, the observed baseline RMS of 5×10^{-10} cm^{-1} will also allow investigation of very weak spectral signals of molecular ions.

Acknowledgments

This work was funded by the NASA Laboratory Astrophysics Grant NNG05GE59G, an ACS Petroleum Research Fund starter grant, and a Camille and Henry Dreyfus New Faculty Award. We gratefully acknowledge Matthew Zwier for development of the data acquisition code, Brian Pohrte for his assistance in constructing the spectrometer, and Brian Brumfield for designing and constructing the Herriott cell. We thank Christopher Tarsitano and Takeshi Oka for sharing the Mathematica spectral fitting routine, and Christopher Morong and Christopher Neese for providing the multiple-Gaussian line-fitting routine. We also thank the referee, Kevin Lehmann, for his many useful suggestions to improve the manuscript.

References

[1] D.W. Ferguson, K.N. Rao, P.A. Martin, G. Guelachvili, J. Mol. Spectrosc. 153 (1992) 599–609.
[2] W.H.J. Childs, Proc. R. Soc. London A 137 (1932) 641–661.
[3] A.B. Meinel, Ap. J. 112 (1950) 562–563.
[4] F.W. Dalby, A.E. Douglas, Phys. Rev. 84 (1951) 843.
[5] C.G. Tarsitano, T. Oka, J. Mol. Spectrosc. 219 (2003) 263–270.
[6] D. Romanini, A.A. Kachanov, N. Sadeghi, F. Stoeckel, Chem. Phys. Lett. 264 (1997) 316–322.
[7] J.B. Dudek, P.B. Tarsa, A. Velasquez, M. Wladyslawski, P. Rabinowitz, K.K. Lehmann, Anal. Chem. 75 (2003) 4599–4605.
[8] G. Berden, R. Peeters, G. Meijer, Int. Rev. Phys. Chem. 19 (2000) 565–607.
[9] D. Collet, J.-L. Destombes, I. Hadj Bachir, T.R. Huet, Chem. Phys. Lett. 286 (1998) 311–316.
[10] D. Halmer, G. von Basum, P. Hering, M. Mürtz, Rev. Sci. Instrum. 75 (2004) 2187–2191.
[11] P.J. Fox, R.E. Scholten, M.R. Walkiewicz, R.E. Drullinger, Am. J. Phys. 67 (1999) 624–630.
[12] J.P. DiGangi, B.S. Thesis, University of Illinois at Urbana-Champaign, http://bjm.scs.uiuc.edu/pubs/DiGangi_thesis.pdf, (2006).
[13] C.M. Lindsay, Ph.D. Thesis, University of Chicago (2002).
[14] B.H. Pate, K.K. Lehmann, G. Scoles, J. Chem. Phys. 95 (1991) 3891–3916.
[15] L.S. Rothman, D. Jacquemart, A. Barbe, D.C. Benner, M. Birk, L.R. Brown, M.R. Carleer, C. Chackerian Jr., K. Chance, L.H. Coudert, V. Dana, V.M. Devi, J.-M. Flaud, R.R. Gamache, A. Goldman, J.-M. Hartmann, K.W. Jucks, A.G. Maki, J.-Y. Mandin, S.T. Massie, J. Orphal, A. Perrin, C.P. Rinsland, M.A.H. Smith, J. Tennyson, R.N. Tolchenov, R.A. Toth, J. Vander Auwera, P. Varanasi, G. Wagner, J. Quant. Spectrosc. Rad. Trans. 96 (2005) 139204.
[16] G.H. Dieke, D.F. Heath, Johns Hopkins Spectroscopic Report 17 (1959).
[17] B.J. McCall, T. Oka, J. Chem. Phys. 113 (2000) 3104–3110.
[18] T.A. Miller, T. Suzuki, E. Hirota, J. Chem. Phys. 80 (1984) 4671–4678.
[19] L.T. Earls, Phys. Rev. 48 (1935) 423–424.
[20] W.C. Ho, W. Jäger, D.T. Cramb, I. Ozier, M.C.L. Gerry, J. Mol. Spectrosc. 153 (1992) 692–700.
[21] Wolfram Research, Inc., Mathematica, Version 5.2, Champaign, IL (2005).
[22] R.Z. Martínez, M. Metsälä, O. Vaittinen, T. Lantta, L. Halonen, J. Opt. Soc. Am. B 23 (2006) 727–739.